Part 3—Spectroscopy, Kinetics, and Quantum Chemistry of the Hydroxymethylperoxy Radical ($HOCH_2OO•$, HMP)

Chapter 4—The OH Stretch and A-X Electronic Cavity Ringdown Spectra of the Hydroxymethylperoxy Radical ($HOCH_2OO•$)

Abstract

The reactions of HO_2 with carbonyl compounds have been proposed to be a sink for carbonyl compounds in the upper troposphere/lower stratosphere. The reaction of HO_2 with the simplest carbonyl, formaldehyde (HCHO), proceeds at room temperature, and thus serves as a prototype for this class of reactions. HO_2 and HCHO first form a hydrogen bound complex before isomerizing into the hydroxymethylperoxy radical ($HOCH_2OO•$, or HMP). Considerable uncertainty exists on the reaction rate of HO_2 + HCHO, underscoring the need to find clean spectroscopic bands of HMP. **In this chapter, we report the ν_1 (OH stretch) and A-X electronic cavity ringdown spectra of the HMP radical.** HMP was formed from the reaction of HCHO with HO_2, using Cl_2 photolysis in the presence of HCHO as the HO_2 source. HMP was detected 100 μs after photolysis. The ν_1 band of HMP is centered at 3622 cm^{-1} with strong and broad P and R branches. Careful selection of experimental conditions minimizes interference from H_2O_2, HCOOH, and $HOCH_2OOH$. Rotationally resolved electronic transitions of HMP were detected at 7391 cm^{-1} (A-X origin), 7561 cm^{-1} (combination band with the OOCO torsion), 7719 cm^{-1} (combination band with OOCO torsion overtone), and 7275 cm^{-1} (hot band of the OOCO torsion). The band assignments are made on the basis of the quantum chemistry calculations presented in Chapter 5, and the observed positions are in excellent agreement with the predicted values.

Introduction

The reactions of the hydroperoxy radical (HO_2) with carbonyl compounds (RC(=O)R') are interesting and important from both an atmospheric chemistry perspective as well as a chemical physics perspective. More than 30 years of experimental[17, 23-26, 96-103, 18, 104-107] and theoretical studies[19-22, 107-112] on this class of reactions have been performed. The basic picture that has evolved is that these reactions become more important at reduced temperatures; in other words, the rate of these reactions increases as temperature decreases. In the Upper Troposphere/Lower Stratosphere (UTLS), a boundary between atmospheric layers with temperature of 200–220 K, the reactions of HO_2 with carbonyl compounds are believed to be a major sink for both HO_2 and carbonyl compounds.[17, 19, 20] Most of the previous studies have focused on the formaldehyde (HCHO), the smallest carbonyl compound.[17, 21, 24-26, 96, 98-100, 102, 103, 109, 110] More recent studies have examined both acetaldehyde (CH_3CHO) and acetone (CH_3COCH_3).[19, 20, 22, 23, 97, 108]

The experimental and theoretical studies on HO_2 + HCHO paint a consistent picture of the reaction mechanism (Reaction 4.1). All of the experimental studies observe an increase in rate with decreasing temperature. This observation implies that the reaction has a negative activation energy: in other words, an intermediate chemical complex [HO_2---HCHO] is formed that is of lower energy than the reactants. Theoretical studies show that the most stable intermediate is formed by two hydrogen bonds, with the hydrogen of HO_2 bound to the carbon of HCHO, and the terminal oxygen of HO_2 bound to a hydrogen on HCHO. For this complex, HO_2 and HCHO lie in the same plane. The best available calculations place this complex 5–7 kcal mol^{-1} below the reactants.[21] The

hydrogen bound complex then isomerizes, with an activation energy that is lower than the dissociation energy of the complex (3–4 kcal mol^{-1}).[21] The final isomerization product is the hydroxymethylperoxy radical, $HOCH_2OO•$, or HMP, and is more stable than the complex (−17 kcal mol^{-1} compared to the reactants).[21]

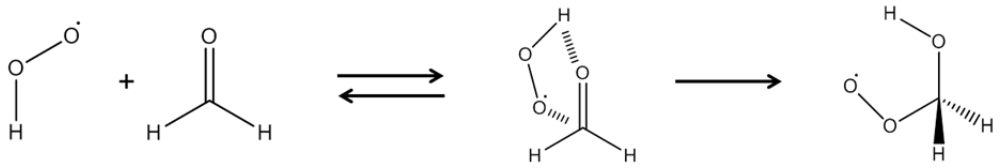

(4.1)

In contrast to reaction with HCHO, the studies on the reactions of HO_2 with CH_3CHO (Reaction 4.2) and CH_3COCH_3 (Reaction 4.3) do not yet paint a consistent picture. Theoretical studies have identified the most likely candidates for the intermediate complexes and the products. Unlike the HCHO case, both the [HO_2---CH_3CHO] and [HO_2---CH_3COCH_3] complexes are not planar: the HO_2 radical is out of plane from the carbonyl molecule.[22]

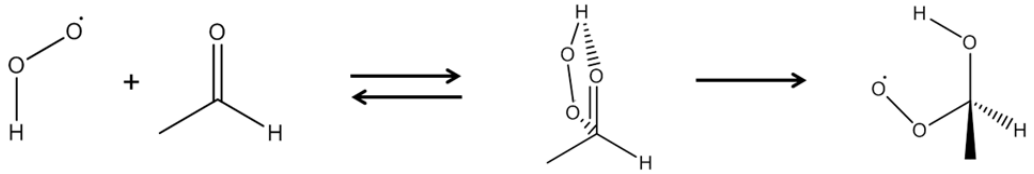

(4.2)

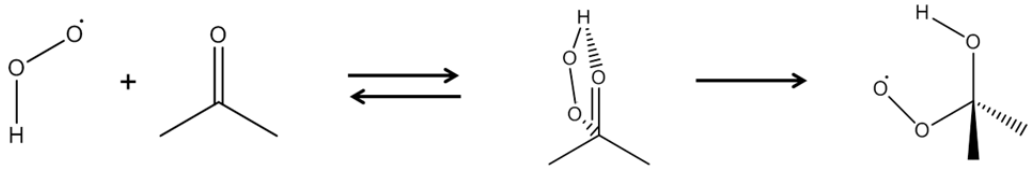

(4.3)

A far more disturbing departure from the HCHO case is that the theoretical studies have not yet come to a consensus as to whether the isomerization reaction's activation energy is higher or lower than the complex's dissociation energy. This has far reaching consequences: kinetic rate constants cannot be predicted accurately. In fact, the two theoretical studies on HO_2 + CH_3COCH_3 predict rate constants that differ by four

orders of magnitude.[19, 22] It is therefore unsurprising that to date, nobody has been able to detect the products of either reaction. With such large uncertainties on the reaction's rate constants, it is impossible to predict whether either reaction will be atmospherically relevant. Gierczak et al. examined the reactions of HO_2 with various ketones, and observed rates of reaction at 298 K that are atmospherically insignificant (less than 10^{-15} cm^3 $molec^{-1}$ s^{-1}).[97] Recent experimental studies by Grieman et al. suggest that at reduced temperature, reactions of HO_2 with ketones are important; their kinetics data show that the rate of HO_2 disappearance significantly increases in the presence of acetone.[23] Grieman's study cannot yet determine whether this effect can be attributed to a reaction of HO_2 with acetone similar to the reaction of HO_2 with HCHO.

Ideally, we would like to design a highly sensitive experiment that could determine whether or not HO_2 will react with acetaldehyde or acetone, and what the kinetic rate constants will be. In order to choose an appropriate method, it is best to first examine HO_2 + HCHO, a reaction that is known to proceed to completion even at room temperature. The first studies on HO_2 + HCHO by Su et al. in 1979[99] made use of end-product analysis by FTIR detection of the stable end-products hydrogen peroxide (Reaction 4.4), hydroxymethylhydroperoxide ($HOCH_2OOH$, or HMHP, Reaction 4.5), formic acid (HCOOH), and methanediol ($HOCH_2OH$, pathways described by Reactions 4.6–4.9).

$$HO_2 + HO_2 \xrightarrow{(+M)} H_2O_2 + O_2 \qquad (4.4)$$

$$HOCH_2OO\bullet + HO_2 \longrightarrow HOCH_2OOH + O_2 \qquad (4.5)$$

$$HOCH_2OO\bullet + HO_2 \longrightarrow O_2 + HCOOH + H_2O \qquad (4.6)$$

$$HOCH_2OO\bullet + HOCH_2OO\bullet \longrightarrow HCOOH + HOCH_2OH + O_2 \qquad (4.7)$$

$$HOCH_2OO\bullet + HOCH_2OO\bullet \longrightarrow HOCH_2O\bullet + HOCH_2O\bullet + O_2 \quad (4.8)$$

$$HOCH_2O\bullet + O_2 \longrightarrow HCOOH + HO_2\bullet \quad (4.9)$$

By combining end-product measurements with a kinetics model, Su et al. were able to back out a kinetic rate constant for HO_2 + HCHO on the order of 10^{-14} cm^3 $molec^{-1}$ s^{-1}. Their detection of HMHP and HCOOH was a good indication that HMP was being formed. However, the rate constant for formation of HMP was subject to large uncertainties because their rate constant for HMP formation was dependent on every other rate constant in the kinetics model.

Any end-product study of HMP kinetics will suffer from two problems. The first problem is that assumptions must be made regarding individual rate constants entered into the kinetics model. Additionally, important reactions may be missing from the model, or assumed to be negligible. Any errors or uncertainties on the kinetics model being used will lead to a derived rate constant that is incorrect or subject to large errors. The second problem is that no verification of a proposed mechanism can be made. If end-product studies are the only experiments performed, then there is no way to confirm that Reactions 4.1–4.9 actually proceed as proposed.

One way to avoid the additional uncertainties inherent in any end-product analysis is to directly detect the HMP radical. Veyret et al. and Burrows et al. performed two such studies in 1989.[25, 26] These studies measure the B-X electronic transition of the HMP radical, centered around 230 nm. The observed transition is very broad, structureless, and has a very large width (full width half maximum of approximately 80 nm). All peroxy radicals exhibit this characteristic B-X electronic transition: a very broad peak centered at 220-240 nm. An example of this is shown in Figure 4.1, which contains the B-X spectra

of HO_2 and methyl peroxy. These spectra look qualitatively similar to the B-X spectrum of HMP. Because all peroxy radicals absorb in the same region, it is very difficult to decouple individual spectra from each other. Additionally, many other molecules, such as the end-product $HOCH_2OOH$, will also absorb in the UV.[113] This may cause further spectral interference.

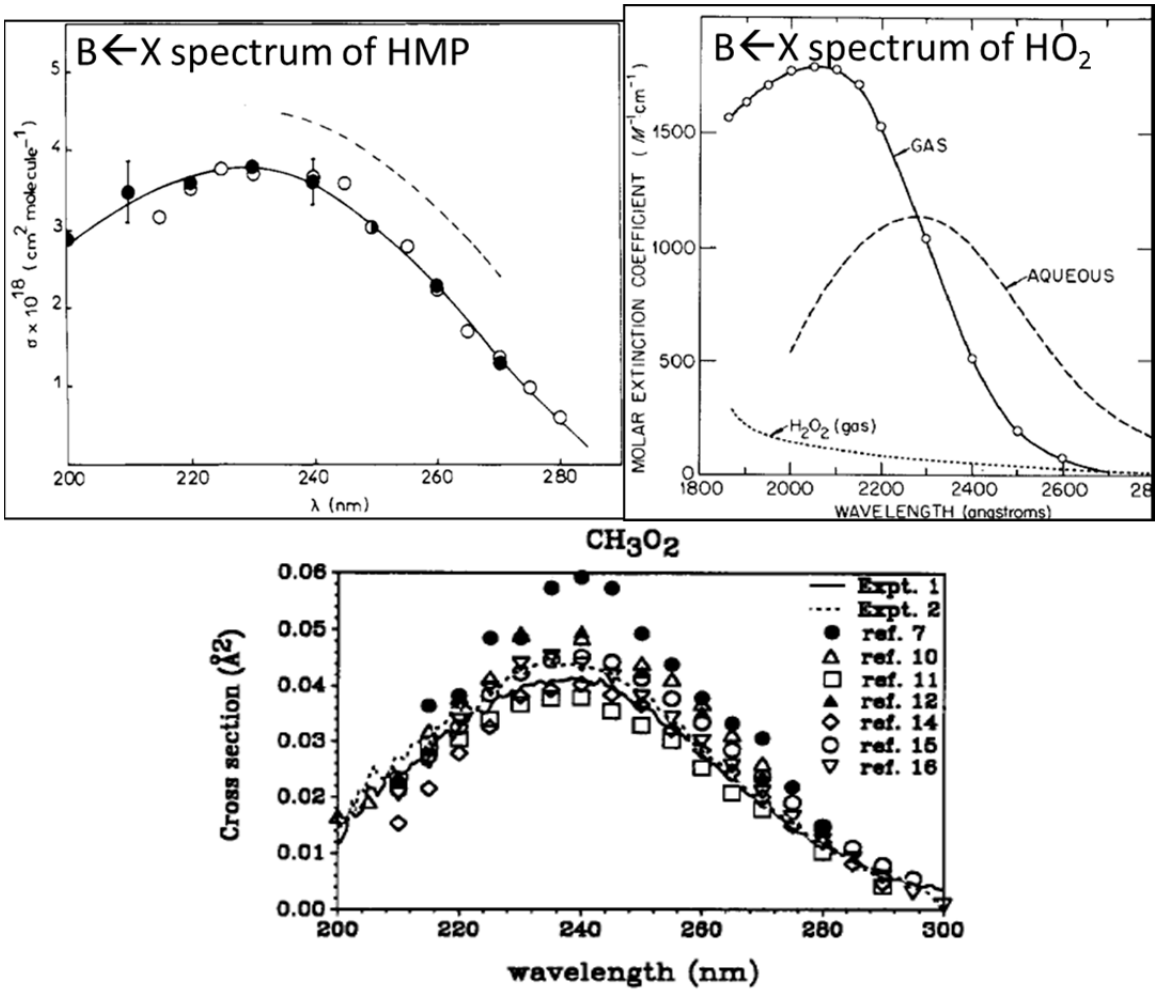

Figure 4.1. B-X spectra of HMP,[26] HO_2, [35] and CH_3OO.[114] All of the spectra exhibit broad absorptions in the region 200-280 nm. HMP B-X spectrum and CH_3OO B-X spectrum are reprinted with permission from Veyret et al. [26] and Maricq et al. [114] respectively. Copyright 1989 and 1992 American Chemical Society. HO_2 B-X spectrum reprinted with permission from Hochanad *et al*. [35] Copyright 1972, American Institute of Physics.

It is unsurprising that the rate constant of HO_2 + HCHO suffers from a somewhat large uncertainty, although far less than for HO_2 and larger carbonyls. Veyret and Burrows report a rate constant for HO_2 + HCHO of $k_1 = 7.7 \times 10^{-15} \times \exp[(625 \pm 550) / T]$ cm^3 $molec^{-1}$ s^{-1}, or $k_1(298\ K) = (6.3[+33.4, -5.3]) \times 10^{-14}$ molec cm^{-3}.[25, 26] The current recommendation by the NASA/JPL kinetics panel recommends a rate constant of $k_1 = 6.7 \times 10^{-15} \times \exp[600 / T]$ cm^3 $molec^{-1}$ s^{-1}, or $k_1(298\ K) = 5.0 \times 10^{-14}$ molec cm^{-3}, with a factor of 5 uncertainty.[27] In order to gain a better understanding of important HO_2 + carbonyl is in the atmosphere, we must first start by reducing the uncertainty in the rate constant of HO_2 + HCHO.

Direct spectroscopic detection through bands unique to $HOCH_2OO$• would pave the way to making a more precise measurement of the rate constant of HO_2 + HCHO than currently available. Until this point, only the B-X spectrum of $HOCH_2OO$• has been within reach because of its large absorption cross section ($\sigma_{peak} = 3.5 \times 10^{-18}$ cm^2 $molec^{-1}$), allowing for ease of detection despite the relatively few $HOCH_2OO$• radicals formed (on the order 10^{13}–10^{15} molec cm^{-3}).

As described in Chapter 2, our pulsed cavity ringdown spectroscopy (CRDS) can detect absorbances as low as 0.1 ppm, allowing for detection of much weaker bands of these radical species ($\sigma_{peak} = 10^{-21}$–10^{-20} cm^2 $molec^{-1}$). Thus, we are not limited to the UV transitions of HMP, we can search for other spectroscopic bands.

The structure of $HOCH_2OO$• suggests two possible bands to measure: the ν_1 (OH stretch) band located in the mid-IR (3600-3700 cm^{-1}), or the A-X electronic band (7000–8000 cm^{-1}). Each of these spectroscopic bands carries with it an advantage and a disadvantage. The ν_1 band is typically a broad and relatively strong band, and has been

used in our group for studies of HOONO (Chapter 3) and alkoxy isomerization (Chapters 7–10).[12, 29-31] For example, the peak cross section of the ν_1 band (P/R branch) of methanol is 6×10^{-20} cm^2 molec cm^{-1}.[40] Although this is a factor of 50 weaker than the B-X transition of $HOCH_2OO$•, the detection limit of methanol (a similar molecule) using CRDS is only 1.6×10^{12} molecules cm^{-3} Hz$^{-½}$. It is relatively easy to generate an equivalent amount of $HOCH_2OO$• during an experiment. However, the disadvantage to using the ν_1 band is that any molecule containing an OH stretch mode will absorb in the same region as $HOCH_2OO$•, notably H_2O_2 formed from Reaction 4.4 and HMHP formed from Reaction 4.5. If the initial experimental conditions are chosen improperly or if products are measured at long times after $HOCH_2OO$• formation, the ν_1 spectrum will become contaminated.

All peroxy radicals have a characteristic A-X electronic transition in the near-IR (7000–8000 cm^{-1}), with the exact position dependent on the structure and functional groups of the peroxy radical.[44] Smaller peroxy radicals, such as methyl and ethyl peroxy, have a series of sharp band heads representing the electronic origin and combination bands of each conformer of the radical. The bandheads are clearly distinct from each other (i.e., different positions and shapes for HO_2, CH_3OO•, $C_2H_5O_2$•, etc.), and thus should provide a unique measure of [$HOCH_2OO$•] over a large range of experimental conditions and times. The main disadvantage is that the A-X bandhead is very weak (for example, $\sigma_{peak}(C_2H_5OO\text{•}, \text{A-X}) = 5.29 \times 10^{-21}$ cm^2 molec^{-1}, giving a detection limit on our CRDS apparatus of 2×10^{13} molec cm^{-3} Hz$^{-½}$).[115] Thus, a larger [$HOCH_2OO$•] is required for detection and subsequent kinetics measurements using the A-X band compared to using the ν_1 band.

A final consideration that must be taken into account is the effect of internal hydrogen bonding on the spectra of $HOCH_2OO•$. Anglada et al. carried out electronic structure calculations on the HO_2 + HCHO potential energy surface, including one conformer of $HOCH_2OO•$.[21] Though not explored in the text, the calculated geometry of $HOCH_2OO•$ suggests a weak intramolecular hydrogen bond, with the distance between the OH and OO• groups about 2.5 Å. If there is a hydrogen bond, the effects on HMP spectroscopy must be considered. Our spectroscopic and computational studies on HOONO (Chapter 3) clearly show that internal hydrogen bonding will shift the ν_1 frequency and possibly lead to sequence band formation (defined as ν_1 intensity outside of the main absorption band due to torsional excitation breaking or strengthening the hydrogen bond).[43] Furthermore, the hydrogen bond lowers some of the electronic energy levels of HMP, and may therefore have an effect on the A-X transition frequency. Finally, it is possible that not all of the HMP in our experiment will be hydrogen bound; the hydroxyl and peroxy groups can be rotated away from each other to yield conformers without hydrogen bonding. All of the above possibilities may affect the position, width, and intensity of the ν_1 and A-X bands that we seek to measure.

Part 3 of this thesis (Chapters 4–6) describes the cavity ringdown spectroscopy, quantum chemistry, and kinetics of the hydroxymethylperoxy radical ($HOCH_2OO•$, HMP), the primary isomerization product of the HO_2 + HCHO reaction. This chapter (Chapter 4) describes the first detection of the ν_1 and A-X bands of HMP via cavity ringdown spectroscopy. Similar to previous experiments,[25, 26] we generate HMP by reaction of HCHO with HO_2, formed through photolysis of Cl_2 in the presence of HCHO and O_2. Cavity ringdown spectroscopy was used to measure the resulting mid-IR and

near-IR spectra over the ranges 3500-3700 cm^{-1} (ν_1) and 7100-8000 cm^{-1} (A-X), 100 μs after photolysis. We show in this chapter that under our experimental conditions these bands provide a clean, unique measurement of HMP. The bands are compared to simulated spectra, and the agreement between experiment and simulation helps verify our assignment of the spectra.

The remaining chapters in Part 3 describe electronic structure calculations and kinetics measurements of HMP. 2-dimensional potential energy surfaces, calculated transition frequencies, and an assessment of appropriate levels of theory for calculations of hydroxylated peroxy radicals are presented in Chapter 5. The kinetics of HMP formation and destruction, measured by the ν_1 and A-X bands, are presented in Chapter 6.

Methods

Apparatus and Chemicals

The cavity ringdown spectrometer, laser system, and gas kinetics flow cell have been described in detail in Chapter 2 (Figures 2.5, 2.7, 2.8), and only a brief summary of the mid-IR (MIR) and near-IR (NIR) configurations is presented here.

Tunable MIR light used to measure the ν_1 spectrum was generated using an optical parametric amplifier. For 65 mJ of 532 nm light and 4–12 mJ of tunable red light (620–665 nm), 0.6–0.8 mJ of tunable infrared light was generated (2900–3800 cm^{-1}). The infrared light was sent into an optical cavity consisting of two highly reflective mirrors (Los Gatos Research, 2.8 μm peak, R = 99.98%). Ringdown traces were collected with a liquid nitrogen cooled InSb detector (Judson J10D-M204-R01M-60) connected to a voltage amplifier (Analog Modules 351A-3) and PC oscilloscope card (GageScope

CS1450). 80 μs of ringdown data were collected per shot, and 16 ringdowns were collected and averaged before being fit. The first eighth of the ringdown lifetime was removed before the data were refit in order to eliminate errors caused from noise near the peak of the ringdown.

Tunable NIR light used to measure the spectrum (6900-8500 cm^{-1}, 100 μJ/pulse) was generated by sending the output from a Nd:YAG (532 nm, 370 mJ/pulse) pumped dye laser (DCM, Rh 640, or Rh 610 dye, 590–660 nm, 40 mJ/pulse peak) into a H_2 filled Raman shifter. The infrared light was sent into an optical cavity consisting of two highly reflective mirrors (Los Gatos Research, 1.35 or 1.20 μm peak, R = 99.98% or 99.99%). Ringdown traces were collected with an amplified InGaAs detector (ThorLabs PDA400) connected to a PC oscilloscope card (GageScope CS1450). 80 μs of ringdown data were collected per shot, and 16 ringdowns were collected and averaged before being fit. The first 1/20 of the ringdown lifetime was removed before the data were refit in order to eliminate errors caused from noise near the peak of the ringdown.

The hydroxymethylperoxy radicals ($HOCH_2OO•$, HMP) measured in this experiment were generated by photolysis of Cl_2 in the presence of HCHO and O_2 (Reactions 4.10–4.12 and 4.1). Photolysis was initiated by 351 nm light from the excimer laser described in Chapter 2. The absorption cross section of Cl_2 at 351 nm is $\sigma_{351nm} = 1.9 \times 10^{-19}$ cm^2 $molec^{-1}$.[27] For the MIR experiments, the UV flux was kept at 1.8×10^{17} molec cm^{-3}, resulting in 3.2% of the Cl_2 being photolyzed. For the NIR experiments, the UV flux was kept at 4.4×10^{17} photons cm^{-2}, resulting in 8.0% of the Cl_2 being photolyzed.

$$Cl_2 \xrightarrow{h\nu = 351\ nm} Cl• + Cl• \qquad (4.10)$$

$$Cl\bullet + HCHO \longrightarrow HCl + HCO\bullet \quad (4.11)$$

$$HCO\bullet + O_2 \longrightarrow HO_2 + CO \quad (4.12)$$

$$HO_2 + HCHO \longrightarrow HOCH_2OO\bullet \quad (4.1)$$

Cl_2 was introduced to the cell from a gas cylinder consisting of 3.5% Cl_2 in He (Air Liquide or Matheson Tri-Gas). HCHO was introduced to the cell by flowing N_2 gas through a vessel of paraformaldehyde (Sigma-Aldrich, 95%) heated to 110 °C. Heating paraformaldehyde leads to the formation of HCHO monomers and oligomers. To trap the oligomers, the N_2/HCHO gas was sent to a dry ice/acetone trap before being sent to the CRDS cell. This method was verified to produce a consistent [HCHO] (±10% between experiments) as measured by the $2\nu_2$ R branch (3510–3520 cm^{-1})[40] and A-X bands (300–310 nm).[116]

Experimental and Flow Conditions

The majority of ν_1 and A-X spectra were taken at a single set of conditions appropriate for each region. In both regions, [HCHO] was factor of 30–1000 higher than [HO_2], with [HCHO] = 1×10^{17} molec cm^{-3} and [HO_2] = 1×10^{14} molec cm^{-3} (MIR) or 3×10^{15} molec cm^{-3} (NIR). By keeping [HCHO] high, HO_2 is more likely to react with HCHO to form HMP (Reaction 4.1), rather than self-react to form H_2O_2 (Reaction 4.4). Higher [HO_2] was required in the NIR in order to generate the higher [HMP] necessary to detect the weak A-X bands.

The HMP spectra were measured by scanning across a range of frequencies in the MIR (3520–3700 cm^{-1}, step size 0.2 cm^{-1}) and NIR (7100–8000 cm^{-1}, step size 0.1 cm^{-1}) while at a constant time after photolysis of Cl_2 (100 μs). Spectra were also recorded at

longer times after photolysis (1000 μs) under alternate conditions in order to show the formation of end-products.

The experimental conditions for the HMP spectroscopy experiments are summarized in Table 4.1. Gas flows were measured using the flowmeters discussed in Chapter 2. The temperature of the gas kinetics cell was taken to be room temperature: no temperature control of any kind was attempted.

Table 4.1. Experimental conditions (gas flows, photolysis parameters, chemical concentrations, and spectrometer performance) for HMP spectroscopy experiments

	HMP, ν_1 (MIR)	HMP, A-X (NIR)
N_2 Purge Flow – Left Mirror	450 sccm	450 sccm
N_2 Purge Flow – Right Mirror	450 sccm	450 sccm
N_2/HCHO Flow	250 sccm	250 sccm
3.5% Cl_2 / He Flow	14 sccm	170 sccm
N_2 Dilution Flow	1250 sccm	1250 sccm
O_2 Flow	650 sccm	650 sccm
Cell Pressure	300 torr	330 torr
Temperature (room)	293 ± 2 K	293 ± 2 K
Flush Time	30 ms	25 ms
Photolysis Window Length	5 cm	5 cm
Excimer Energy at 351 nm	160 ± 10 mJ/pulse	160 ± 10 mJ/pulse
% Cl_2 Photolyzed	3.2%	8.0%
$[Cl\bullet]_0 \sim [HO_2]_0$	1×10^{14} cm^{-3}	3×10^{15} cm^{-3}
[HCHO]	1×10^{17} cm^{-3}	1.1×10^{17} cm^{-3}
$[O_2]$	2.0×10^{18} cm^{-3}	2.2×10^{18} cm^{-3}
Optical Cell Length	52 cm	52 cm
$1/\tau_0$ (purge only)	1.3×10^5 Hz, 3638 cm^{-1}	1.2×10^5 Hz, 7550 cm^{-1}
$1/\tau$ (background gases)	1.4×10^5 Hz, 3638 cm^{-1}	1.3×10^5 Hz, 7550 cm^{-1}
$\Delta\tau/\tau$[a]	0.34%	0.28%
Sensitivity (2σ)	2.1 ppm Hz$^{-½}$	1.6 ppm Hz$^{-½}$

a) $\Delta\tau/\tau$ reported for averaging 16 ringdown traces per point

The cell flush time, $[Cl_2]$, and $[Cl\bullet]$ are calculated from the experimental parameters Table 4.1. Derivations of these equations are presented in Chapter 8; therefore,

only the final results are presented here. The flush time is defined as the amount of time to remove the chemicals within the photolysis length from the ringdown cavity, and is calculated from Equation 4.13:

$$t_{flush} = \left(\frac{V_{in-out}}{\sum_{flush} f_i} \right) \times \left(\frac{p_{cell}}{p_{st}} \right), \tag{4.13}$$

where t_{flush} is the flush time for the chemical sample, $V_{\text{in-out}}$ is the volume between the inlet for butyl nitrite and vacuum outlet ($V_{\text{in-out}}$ = 3.93 cm^3 for the cell used in these experiments), $\sum_{flush} f_i$ is the total flow rate of gases in the direction of flushing (in sccm), p_{cell} is the pressure in the CRDS cell, and p_{st} is the standard pressure (760 torr).

The fraction of Cl_2 that is photolyzed can be calculated from Equation 4.14:

$$\%_{photolysis} = \frac{\left(P_{excimer} \middle/ A_{meter} \right)}{F_{excimer}} \left(\frac{\lambda}{hc} \right) \left(\sigma_{Cl_2,\lambda} \right) (X) \left(\frac{A_{UV,laser}}{A_{UV,CRDS}} \right), \tag{4.14}$$

where $\%_{\text{photolysis}}$ is the fraction of RONO that is photolyzed, ($P_{\text{excimer}}/A_{\text{meter}}$) is the power per unit area of the UV light (read directly from the power meter), F_{excimer} is the rep rate of the excimer laser (10 Hz), h is Planck's constant, c is the speed of light, λ is the wavelength of the excimer light (351 nm), $\sigma_{\text{Cl2},\lambda}$ is the absorption cross section of Cl_2 at the excimer wavelength (1.9×10^{-19} cm^2 molec^{-1} at 351 nm), X is the quantum yield for photolysis (taken to be 1), $A_{\text{UV,laser}}$ is the area of excimer beam measured at the excimer laser output, and $A_{\text{UV,CRDS}}$ is the area of excimer beam measured at the CRDS cell. For the ν_1 experiment, $\frac{A_{UV,laser}}{A_{UV,CRDS}} = 2$. For the A-X experiment, $\frac{A_{UV,laser}}{A_{UV,CRDS}} = 5$.

Results

We present the results of our spectroscopy study in three parts. First, we discuss the chemistry relevant to our experiment following photolysis of the chlorine. Under each set of experimental conditions, we show that after 100 μs, the majority of products being detected are HMP. Second, we present the ν_1 spectrum at various times after photolysis and $[HO_2]$:[HCHO] ratios. Under our best conditions, we observe a clean HMP ν_1 band centered at 3622 cm^{-1}, with broad P and R branches. Under all conditions, we observe interference from secondary products (HCOOH, H_2O_2, $HOCH_2OOH$), though these can be greatly minimized through a judicious choice of starting conditions and measurement time. Third, we present the A-X spectrum of HMP over the range 7100-8000 cm^{-1}. We observe the origin and many combination/hot bands, assigned on the basis of our quantum chemistry calculations (discussed in detail in Chapter 5). The qualitative shape of the spectrum is similar to methyl peroxy, though relative intensities and band positions are different. In both spectra sections, we compare our experimental spectra to simulated spectra (based on the parameters calculated in Chapter 5). We observe excellent agreement between the experiment and simulation, giving us confidence that we have detected HMP.

Chemistry

Our radical chemistry is initiated by photolysis of Cl_2 with UV light (351 nm, $\sigma_{351} = 1.8 \times 10^{-19}$ cm^2 $molec^{-1}$).[27]

$$Cl_2 \xrightarrow{h\nu = 351\ nm} Cl\bullet + Cl\bullet \qquad (4.15)$$

Simultaneously, HCHO can also photolyze (Reaction 4.16), although this pathway is minor ($\sigma_{351} = 8.9 \times 10^{-22}$ cm^2 molec^{-1}, $\phi_{16} = 0.35$).[27]

$$HCHO \longrightarrow H_2 + CO \quad (4.16)$$

For our photon fluxes, (1.8–4.4) × 10^{17} photons cm^{-2}, only 0.006%–0.014% of the HCHO will photolyze. For [HCHO] = 1×10^{17} molec cm^{-3}, this translates to (5.6×10^{12}–1.4×10^{13}) molec cm^{-3} of HCHO that is photolyzed.

Following photolysis, Cl• reacts rapidly with HCHO to form HCl and HCO• (Reaction 4.17, k_{298K}=7.3×10^{-11} cm^3 molec^{-1} s^{-1}).[27] HCO• then reacts with O_2 to form CO and HO_2 (Reaction 4.18, $k_{298K} = 5.2 \times 10^{-11}$ cm^3 molec^{-1} s^{-1}).[27]

$$Cl\bullet + HCHO \longrightarrow HCl + HCO\bullet \quad (4.17)$$

$$HCO\bullet + O_2 \longrightarrow HO_2 + CO \quad (4.18)$$

For [HCHO] = 10^{17} molec cm^{-3}, the lifetime of Reaction 4.17 is 0.14 μs. For [O_2] = 2×10^{18} molec cm^{-3}, the lifetime of Reaction 4.18 is 10 ns. Therefore, conversion of Cl• to HO_2 can be considered instantaneous compared to the time resolution of our experiment (empty cavity ringdown lifetime of 8 μs).

The vast majority of Cl• is converted to HO_2, the two major side reactions are very slow compared. First, Cl• can react with O_2 to form ClOO• (Reaction 4.19, $k_{298K,300torr} = 2.0 \times 10^{-14}$ cm^3 molec^{-1} s^{-1}, lifetime 25 μs).[27] Second, HCO• radicals can react with Cl_2 (Reaction 4.20, $k_{298K} = 7 \times 10^{-12}$ cm^3 molec^{-1} s^{-1}, lifetime 7 μs).[117]

$$Cl\bullet + O_2 \xrightarrow{+M} ClOO\bullet \quad (4.19)$$

$$HCO\bullet + Cl_2 \longrightarrow \text{products} \quad (4.20)$$

At this point, the HO_2 can undergo one of two reactions: reaction with HCHO to form HMP (Reaction 4.1, $k_{298K} = 5.7 \times 10^{-14}$ cm^3 molec^{-1} s^{-1}, lifetime 175 μs),[25, 26] or

self-reaction to form H_2O_2 and O_2 (Reaction 4.4, $k_{298K,300torr} = 2.0 \times 10^{-12}$ cm^3 molec^{-1} s^{-1}, initial lifetime 2.5 ms in the ν_1 experiment, 80 μs in the A-X experiment).[27] Note that lowering [HCHO]:[HO_2] will cause HO_2 self-reaction to be favored. Since H_2O_2 causes spectral interference in the ν_1 experiment, it is crucial to keep [HCHO] much higher than [HO_2]. Conversely, H_2O_2 does not absorb in the A-X region of HMP, and therefore we do not need to worry about [HCHO]:[HO_2].

$$HO_2 + HCHO \longrightarrow HOCH_2OO\bullet \quad (4.1)$$

$$HO_2 + HO_2 \xrightarrow{+M} H_2O_2 + O_2 \quad (4.4)$$

We now turn our attention to the pathways for HMP destruction. The major pathways for HMP destruction are reaction with HO_2 to form $HOCH_2OOH$ (Reaction 4.21, $k_{298K} = 7.2 \times 10^{-12}$ cm^3 molec^{-1} s^{-1}) or formic acid (Reaction 4.22, $k_{298K} = 4.8 \times 10^{-12}$ cm^3 molec^{-1} s^{-1}), or self-reaction to form either hydroxymethoxy (Reaction 4.23, $k_{298K} = 5.2 \times 10^{-12}$ cm^3 molec^{-1} s^{-1}) or formic acid (Reaction 4.24, $k_{298K} = 7.0 \times 10^{-13}$ cm^3 molec^{-1} s^{-1}). The hydroxymethoxy can react with O_2 to form formic acid (Reaction 4.25, $k_{298K} = 3.5 \times 10^{-14}$ cm^3 molec^{-1} s^{-1}).[25, 26]

$$HOCH_2OO\bullet + HO_2 \longrightarrow HOCH_2OOH + O_2 \quad (4.21)$$

$$HOCH_2OO\bullet + HO_2 \longrightarrow HCOOH + H_2O + O_2 \quad (4.22)$$

$$HOCH_2OO\bullet + HOCH_2OO\bullet \longrightarrow HOCH_2O\bullet + HOCH_2O\bullet + O_2 \quad (4.23)$$

$$HOCH_2OO\bullet + HOCH_2OO\bullet \longrightarrow HCOOH + HOCH_2OH + O_2 \quad (4.24)$$

$$HOCH_2O\bullet + O_2 \longrightarrow HCOOH + HO_2 \quad (4.25)$$

Unimolecular reaction of HMP back to HO_2 + HCHO is too slow to act as a loss mechanism (Reaction 26, lifetime 126 s^{-1}).[25, 26]

$$HOCH_2OO\bullet \longrightarrow HO_2 + HCHO \quad (4.26)$$

We can calculate branching ratios of Reactions 4.1 and 4.4 based on their relative lifetimes, and therefore estimate [HMP] and [H_2O_2] in both the ν_1 and A-X experiments. These values are summarized in Table 4.2, along with conditions for other spectra reported in this chapter. For this calculation, we assume that Reactions 4.1 and 4.4 are the only relevant reactions of HO_2 within the timescale of HMP formation. We expect 94% of HO_2 to be converted to HMP in the ν_1 experiment and 31% in the A-X experiment.

Given the estimated [HMP], we can also estimate the lifetime of HMP in our experiment. These lifetimes are also summarized in Table 4.2, and combine the lifetimes of Reactions 4.21–4.24. For this lifetime calculation, we use the [HO_2] present after the listed lifetime of HO_2 + HCHO for each condition. Because HO_2 is rapidly decreasing over the course of the experiment, we expect that all of the predicted HMP lifetimes are too low.

Table 4.2. Summary of lifetimes (μs), branching ratios, estimated [H_2O_2] (molec cm^{-3}), and estimated [HMP] (molec cm^{-3}) for HO_2 + HO_2 and HO_2 + HCHO reactions under experimental conditions, as predicted by our analysis of chemistry.

Expt	[HO_2]	[HCHO]	$(\tau_{HO2+HO2})_0$	$\tau_{HO2+HCHO}$	BR(HMP)	[H_2O_2]	[HMP]	τ_{HMP}
ν_1[a]	1.0e14	1.0e17	2530	175	93.5%	6.5e12	9.4e13	660
A-X[a]	3.2e15	1.0e17	79	175	31.1%	2.2e15	1.0e15	75
ν_1 #2[b]	1.2e15	5.0e15	211	3509	5.7%	1.1e15	6.8e13	1250
ν_1 #3[b]	2.4e14	9.0e15	1054	1949	35.1%	1.6e14	8.4e13	860
A-X #2[b]	1.5e15	1.0e17	169	175	49.0%	7.6e14	7.4e14	91

a) Conditions for reported spectra
b) Non-optimal conditions leading to unclean spectra or low [HMP]

Based on Table 4.2, we expect to form a detectable [HMP] with minimal interference from [H_2O_2] in the ν_1 region. To confirm this, we constructed a kinetics model using rate constants available in the literature.[27, 117, 118] This kinetics model is summarized in Appendix E, as it is capable of modeling a number of reactions:

HO_2 + (HCHO,NO) and OH + (CO, NO_2, O_2). Table 4.3 summarizes [HO_2], [HCHO], lifetimes, [HMP], and HMP lifetime obtained from the model. We note $\tau_{HO2+HO2}$, $\tau_{HO2+HCHO}$, the branching ratio, [H_2O_2], and [HMP] are in excellent agreement with our chemistry analysis (factor of 3). The lifetime of HMP from the kinetics model is longer than from our chemistry analysis because [HO_2] and [HMP] decrease over time, a factor not included in our simple chemistry analysis.

Table 4.3. Summary of lifetimes (μs), branching ratios, estimated [H_2O_2] (molec cm^{-3}), and estimated [HMP] (molec cm^{-3}) for HO_2 + HO_2 and HO_2 + HCHO reactions under experimental conditions, as predicted by our kinetics model.

Expt	[HO_2]	[HCHO]	($\tau_{HO2+HO2}$)[a]	$\tau_{HO2+HCHO}$	BR(HMP)[b]	[H_2O_2]	[HMP]	τ_{HMP}
ν_1[c]	1.0e14	1.0e17	1480[a]	105	81%	1.6e12	6.8e13	>1000
A-X[c]	3.2e15	1.0e17	59[a]	190	36%	6.2e14	3.5e14	450
ν_1 #2[d]	1.2e15	5.0e15	198[a]	6000[a]	4%	3.9e14	1.8e13	>1000
ν_1 #3[d]	2.4e14	9.0e15	646[a]	2078[a]	40%	4.3e13	2.9e13	>1000
A-X #2[d]	1.5e15	1.0e17	110[a]	220	59%	2.0e14	2.9e14	555

a) Initial lifetime
b) Branching ratio calculated as [HMP] / ([HMP]+[HO_2])
c) Conditions for reported spectra
d) Non-optimal conditions leading to unclean spectra or low [HMP]

Finally, on the basis of our kinetics model, we can find acceptable conditions for our experiments. For the ν_1 experiment, we must generate a large amount of HMP while keeping other species with OH stretches in low concentrations (notably H_2O_2, $HOCH_2OOH$, HCOOH). For the A-X experiment, we simply wish to generate as much HMP as possible. However, large quantities of HO_2 will increase the destruction rate of HMP (Reactions 4.21 and 4.22), and cause the concentration of HMP to vary over our data collection window (80 μs).

Figure 4.2 shows modeled kinetics of HMP and other species with OH groups for the ν_1 and A-X experimental conditions. We observe that the ideal detection time for both systems is 100 μs. This timing satisfies the requirements listed in the previous paragraph.

The rapid growth of HCOOH means that we cannot measure the maximum concentration of HMP in the ν_1 experiment (at 400 μs) without spectral interference.

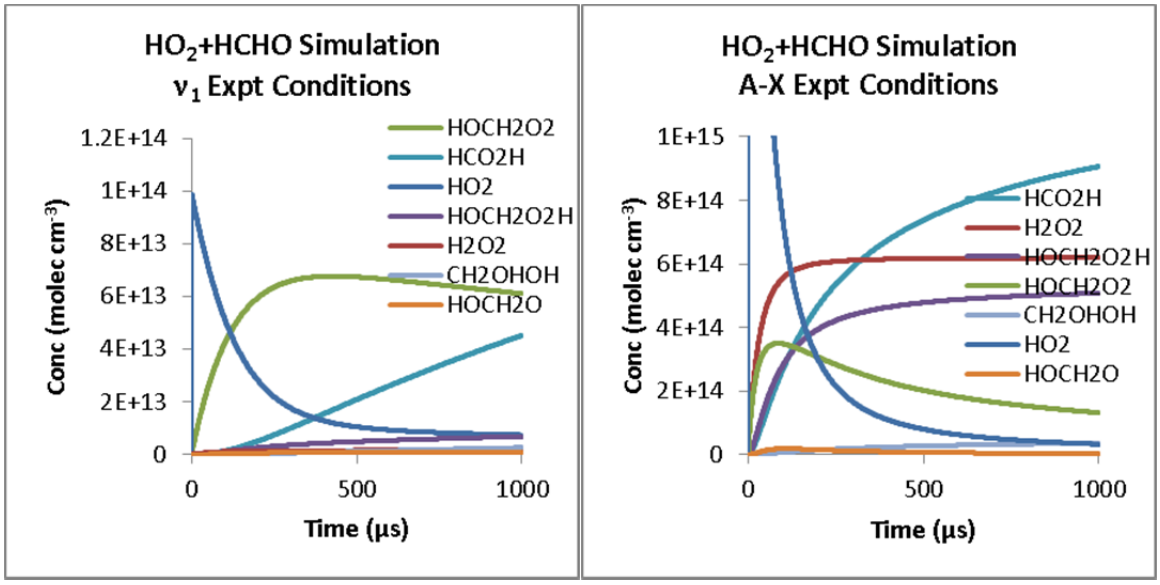

Figure 4.2. Kinetics simulations for our HO_2 + HCHO experiments: ν_1 (left) and A-X (right). Conditions are listed in Table 4.1. In both systems, we make our measurements of HMP at 100 μs.

HMP ν_1 Spectrum

Figures 4.3–4.6 show a series of mid-infrared spectra obtained following the photolysis of Cl_2 in the presence of HCHO and O_2. All spectra were taken with a 0.2 cm^{-1} step size, with different photolysis-probe delay times dependent on experimental conditions (noted with each figure). The spectra presented in Figure 4.3 are unsubtracted (i.e., the mirror reflectivity and absorption by the background gases have not been subtracted out). Figures 4.4–4.6 have had the background spectra in the absence of photolysis (excimer off) subtracted.

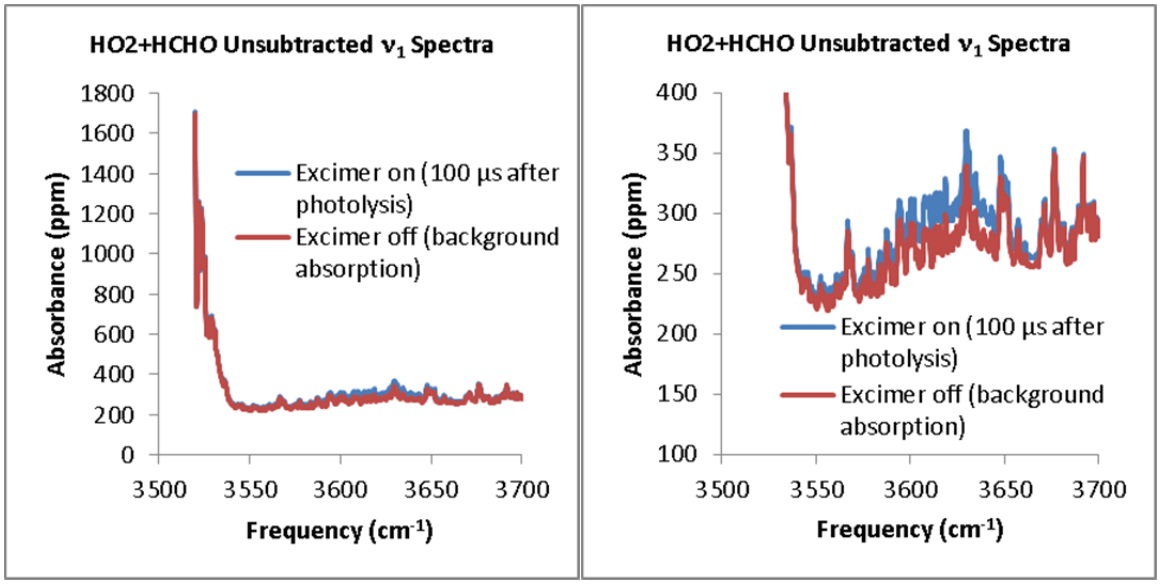

Figure 4.3. Cavity loss (mirror reflectivity plus absorption) of the precursor chemicals (excimer off) and the photolysis products (excimer on) in the mid-IR for Cl_2 in the presence of HCHO and O_2. The right panel zooms in on the region 100–400 ppm to better illustrate those absorption features. The spectrum was taken at room temperature (295 ± 2 K) and $[O_2] = 2 \times 10^{18}$ molec cm^{-3}, 0.2 cm^{-1} between data points. The large absorption at 3500–3540 cm^{-1} is from the $2\nu_2$ band of HCHO. Structured absorption across the entire spectrum is due to background H_2O. Additional absorption features are observed following photolysis of Cl_2.

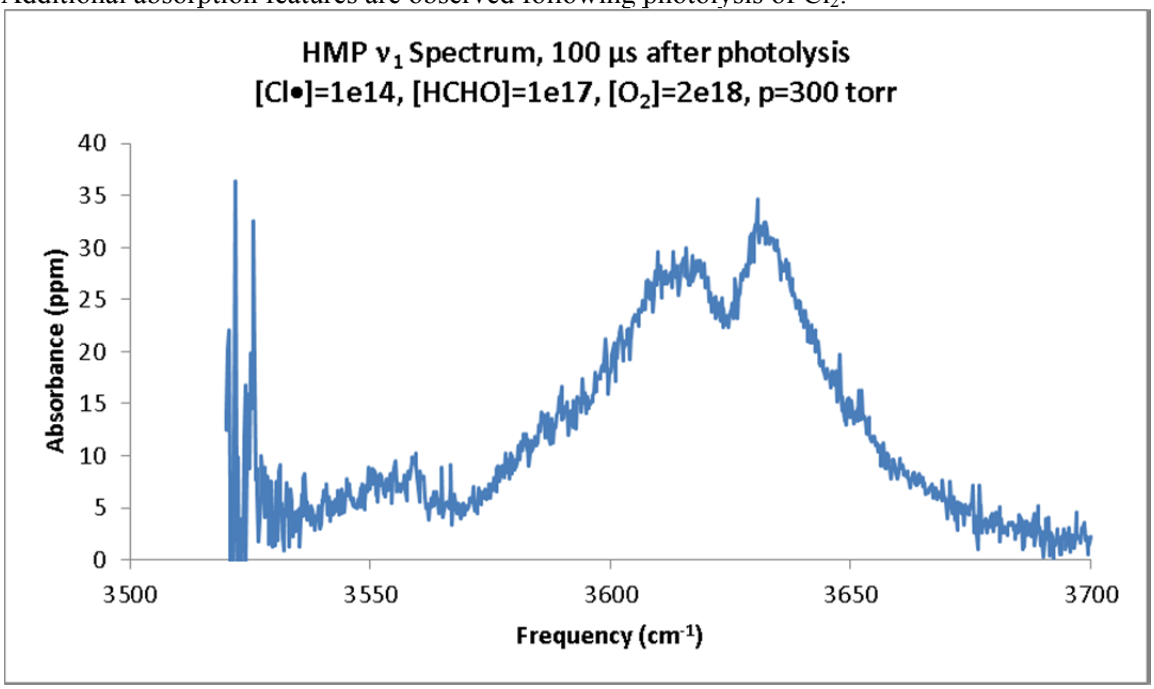

Figure 4.4. ν_1 (OH stretch) spectrum of $HOCH_2OO\bullet$ (HMP), the product of HO_2 + HCHO, taken under our most ideal conditions. The spectrum was recorded at 295 K, 300 torr, 0.2 cm^{-1} between data points, 100 µs after generation of HO_2, $[HO_2] = 1 \times 10^{14}$ molec cm^{-3}, $[HCHO] = 1 \times 10^{17}$ molec cm^{-3}. The spectrum was signal averaged for 6.4 s per point. Based on our kinetics model, we predict $[HMP]:[H_2O_2] = 39$ and $[HMP]:[HCOOH] = 30$

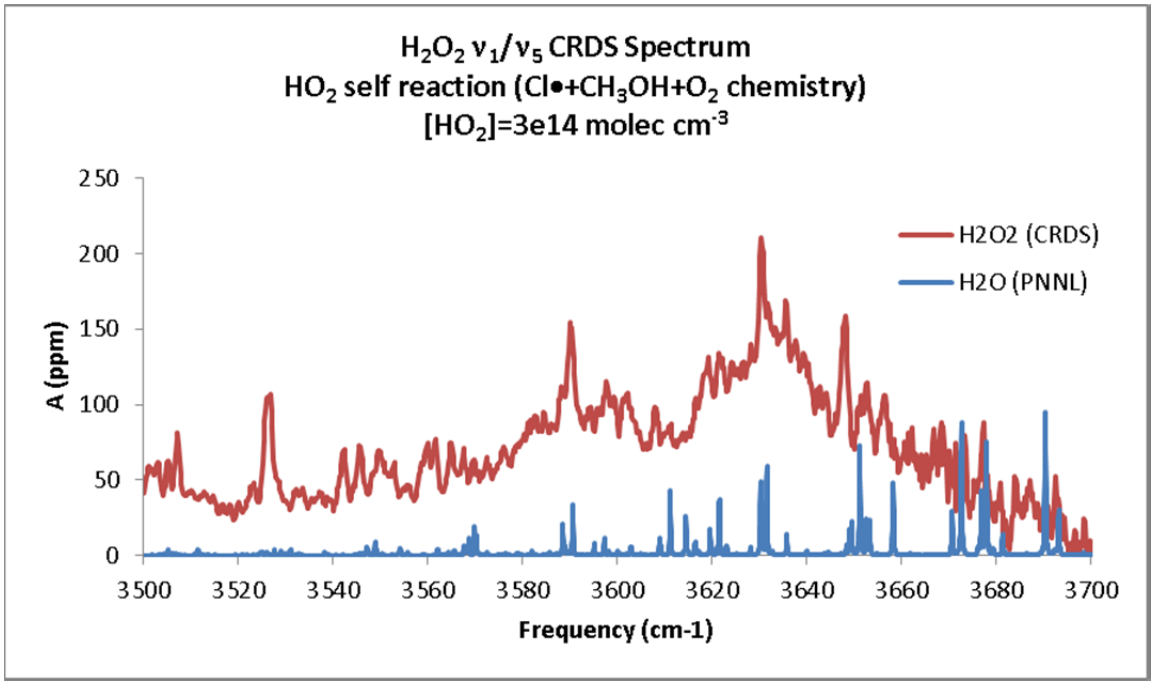

Figure 4.5. ν_1/ν_5 (OH stretch) spectrum of H_2O_2, formed from HO_2 self-reaction. HO_2 was generated by Cl• + CH_3OH + O_2 chemistry. [Cl•]=3 × 10^{14} molec cm^{-3}, [CH_3OH] = 1 × 10^{15} molec cm^{-3}, [O_2] = 2 × 10^{18} molec cm^{-3}, p = 300 torr, 0.2 cm^{-1} step size. The spectrum is a composite of five scans (8.0 s average per point), ranging from 100–1000 μs after Cl_2 photolysis. Spectral interference from CH_3OH loss has been subtracted out of the CRDS spectrum. A reference spectrum of H_2O[40] has been overlaid to indicate which peaks belong to water rather than H_2O_2. We note that the spectrum of H_2O_2 is qualitatively different than the HMP spectrum in Figure 4.4.

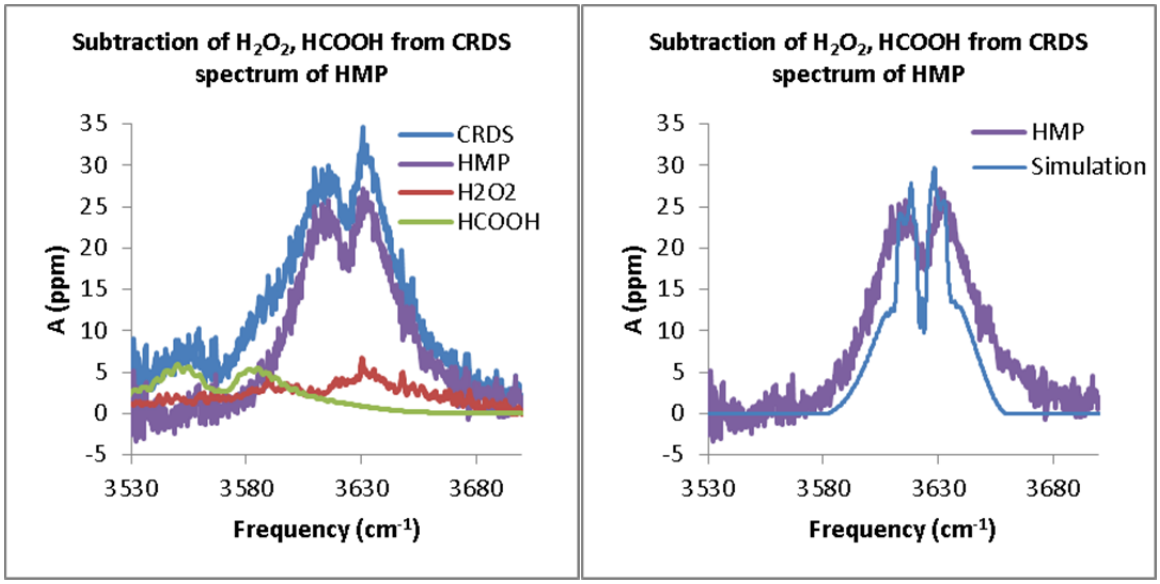

Figure 4.6. Left: Subtraction of H_2O_2 and HCOOH from the cavity ringdown spectrum to obtain the pure ν_1 spectrum of HMP. The integrated absorbance of the subtracted HMP ν_1 band is 1.3×10^{-3} cm^{-1}. Assuming the B3LYP integrated cross section 8.8×10^{-18} cm $molec^{-1}$, we estimate [HMP] = 3.1×10^{13} molec cm^{-3}, in excellent agreement with our kinetics model (4.2×10^{13} molec cm^{-3}). Right: Comparison of the ν_1 spectrum of HMP to simulation, B3LYP/6-31+G(d,p), anharmonic rotational constants. We observe good agreement between the CRDS and simulated ν_1 bands.

Figure 4.3 shows the background IR spectra of the reactants (excimer off) and the IR spectra of the background plus signal (excimer on). At frequencies less than 3540 cm^{-1}, the spectrum is dominated by the $2\nu_2$ band of HCHO. To better show the rest of the absorptions in this region, the right panel zooms in to absorptions of less than 400 ppm. We notice sharp peaks across the entire region, attributed mainly to residual water from the paraformaldehyde sample. Some of the peaks are likely also from HCHO.[40]

Following photolysis of Cl_2 at 351 nm, an additional absorption is observed over the range 3550–3700 cm^{-1}. Figure 4.4 shows the IR spectrum of the products formed under the experimental conditions in Table 4.1, 100 μs after photolysis of Cl_2 in the presence of HCHO and O_2. We observe a clear peak centered at 3622 cm^{-1}, with broad P and R branches (FWHM = 60 cm^{-1}). The shape and position of this band are not

consistent with any of the other molecules discussed in the *Chemistry* section (HCOOH, H_2O_2, $HOCH_2OOH$).[40, 119]

We do observe traces of spectral interference in Figure 4.4. The ν_1 band of HCOOH is clearly visible at 3570 cm^{-1}, although its peak absorbance is a factor of 6 weaker than the main band at 3622 cm^{-1}. There are also small peaks in the region 3645–3655 cm^{-1}. As discussed in the *Chemistry* section, one of the side products in our experiment is H_2O_2, and these peaks belong to the ν_1/ν_5 bands (OH symmetric and antisymmetric stretches) of H_2O_2. To confirm this, we measured the spectrum of H_2O_2 in our CRDS apparatus by generating HO_2 from Cl• / CH_3OH / O_2 chemistry, a "pure" source of HO_2 that will not form appreciable amounts of organic hydroxide species. This spectrum is shown in Figure 4.5. The H_2O_2 peaks match up with the weak peaks in Figure 4.4, indicating a very small amount of spectral interference from H_2O_2.

We can subtract out the contributions from HCOOH and H_2O_2, allowing us to compare the observed band to a simulation of HMP. Combined with our analysis in the *Chemistry* section, this would allow us to assign the observed absorption to the ν_1 band of HMP. Figure 4.6 shows this subtraction and simulation. The subtraction (left panel) was performed in two steps: first scaling the H_2O_2 spectrum to eliminate the peaks in the 3645–3655 cm^{-1} region, then scaling the HCOOH spectrum to eliminate the observed ν_1 band at 3555–3570 cm^{-1}.

The ν_1 band of HMP was simulated using the PGopher program.[120] The geometry, dipole derivatives, and anharmonic rotational constants were calculated at the B3LYP/6-31+G(d,p) level of theory and basis using Gaussian 09W.[121] We observe very good agreement between our simulation and the subtracted CRDS band (Figure 4.6, right

panel) with the main difference being that the FWHM of the simulated band (40 cm^{-1}) is narrower than the CRDS band (60 cm^{-1}). This may be due to the internal hydrogen bond formation (discussed in Chapter 5).

We assign the absorption band at 3622 cm^{-1} (Figure 4.4) to the ν_1 mode of HMP for the following two reasons. First, our two analyses in the *Chemistry* section (both from rate constants and from the kinetics model) show that under our experimental conditions, the species in our spectrometer should be mostly HMP. Second, the subtracted CRDS spectrum is in excellent agreement with our simulated ν_1 band (Figure 4.6).

We can use the integrated absorbance of the subtracted spectrum (Figure 4.6) and the theoretical integrated intensity (calculated during our simulation) to estimate [HMP]:

$$[\mathrm{HMP}] = \frac{\int_{3530\ \mathrm{cm^{-1}}}^{3700\ \mathrm{cm^{-1}}} A d\bar{\nu}}{L_{phot} \int \sigma d\bar{\nu}}, \tag{4.27}$$

where $\int_{3530\ \mathrm{cm^{-1}}}^{3700\ \mathrm{cm^{-1}}} A d\bar{\nu}$ is the integrated absorbance of the subtracted band in Figure 4.6 (1.3×10^{-3} cm^{-1}), L_{phot} is the photolysis length (5 cm), and $\int \sigma d\bar{\nu}$ is the integrated cross section from our quantum chemistry calculations (8.8×10^{-18} cm $molec^{-1}$ at B3LYP/6-31+G(d,p)). Using Equation 4.27, we estimate [HMP] = 3.1×10^{13} molec cm^{-3}. This is in excellent agreement with the prediction from our kinetics model, [HMP] = 4.2×10^{13} molec cm^{-3}.

Using these either of concentrations (B3LYP or kinetics model), we can estimate the peak cross section of HMP. This plot is shown in Figure 4.7. It should be noted that these values are very crude estimates due to possible variations in [HCHO], [HO_2], and uncertainty on the absolute [HMP]. Nonetheless, we can estimate the peak cross section

to be on the order of 10^{-19} cm^2 molec^{-1}. This is consistent with other small alcohols such as methanol (8×10^{-20} cm^2 molec^{-1}), ethanol (8×10^{-20} cm^2 molec^{-1}), or 1-propanol (7×10^{-20} cm^2 molec^{-1}).

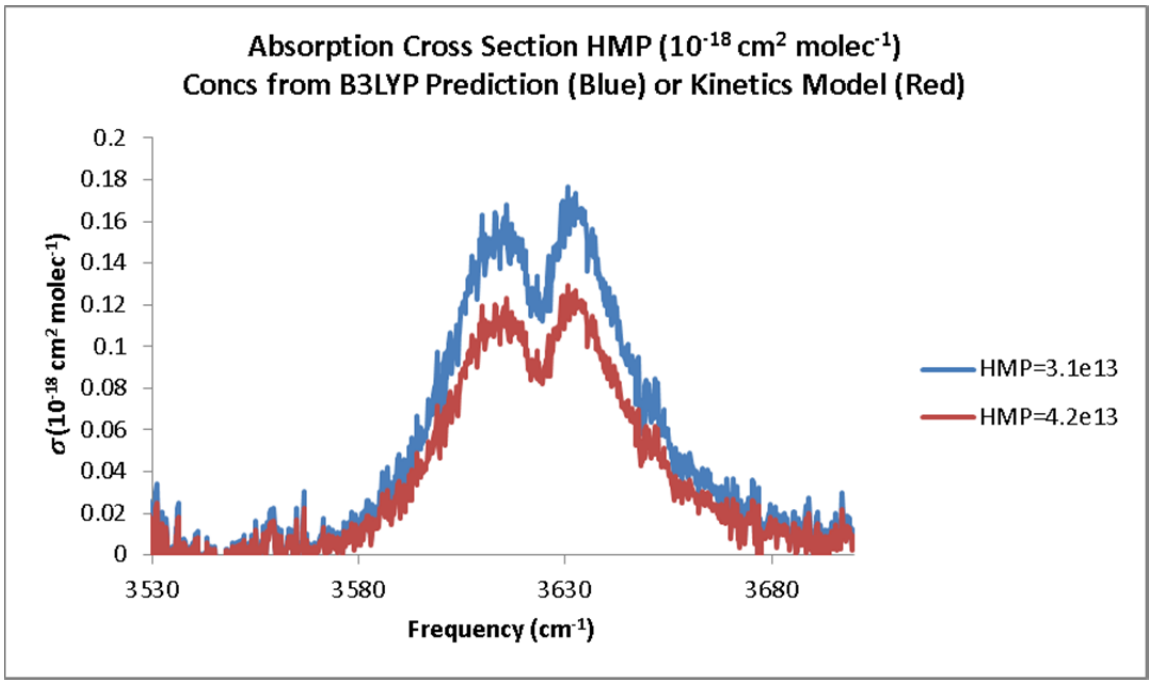

Figure 4.7. Absorption cross sections of the ν_1 band of HMP. The [HMP] used were taken from the B3LYP/6-31+G(d,p) intensity and CRDS integration (blue) and the kinetics model (red).

As mentioned in the *Chemistry* section, incorrect selection of initial conditions, notably the ratio [HCHO]:[HO_2] and the absolute reactant concentrations, will lead to severe spectral interference or large levels of noise. Figure 4.8 shows spectra for poor initial conditions. The left panel uses a very low [HCHO]:[HO_2] ratio compared to Figure 4.4 (4 vs 1000). The right panel uses a somewhat low [HCHO]:[HO_2] ratio (38), but with [HCHO] = 9×10^{15} molec cm^{-3}, a factor of 11 lower than the spectrum in Figure 4.4. At very low [HCHO]:[HO_2] ratios, we observe a broad absorption across the entire region (3500–3700 cm^{-1}), indicative of H_2O_2 formation. In the right panel, we observe essentially the same spectrum as in Figure 4.4, but with much lower peak absorption (and

consequently a lower signal-to-noise ratio). The conclusion that we draw from Figure 4.8 is that we must be careful selecting initial conditions in our experiments, especially OH stretch experiments where secondary/side products will cause significant interference.

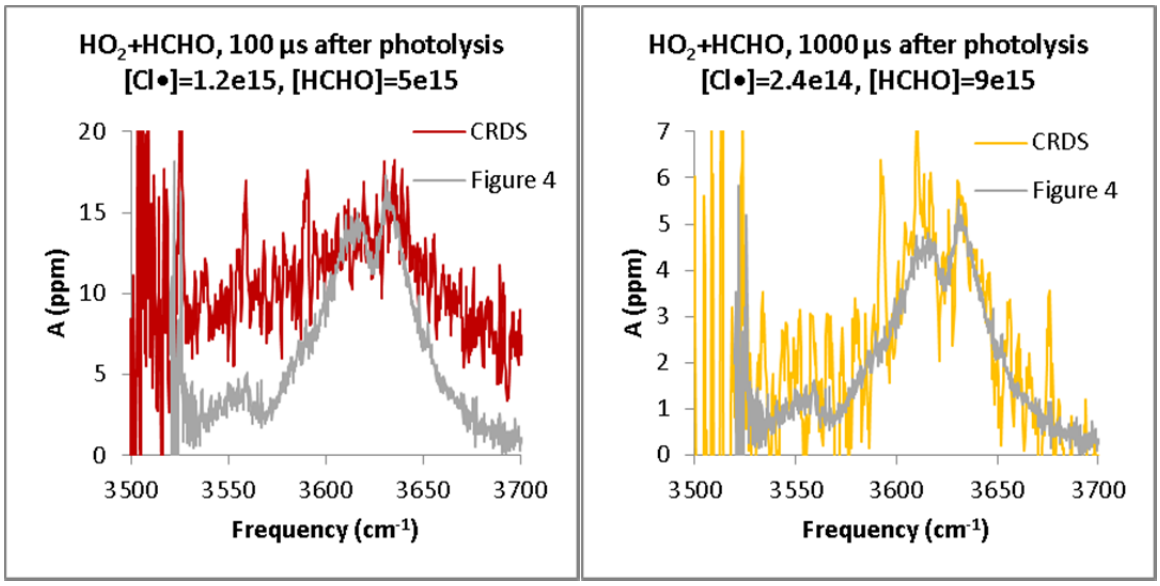

Figure 4.8. ν_1 (OH stretch) spectra of $HOCH_2OO\bullet$ (HMP), the product of HO_2 + HCHO, taken under poor conditions. Left: very low [HCHO]:[HO_2] ratio. Right: Low absolute concentrations. The spectra were recorded at 295 K, 300 torr, 0.2 cm^{-1} between data points. Left: [HO_2] = 1.2 × 10^{15} molec cm^{-3}, [HCHO] = 5 × 10^{15} molec cm^{-3}, 100 µs after HO_2 formation. We observe significant interference from other species (HCOOH, H_2O_2), causing the spectrum to disagree with the spectrum presented in Figure 4.4 (shown in gray). Right: [HO_2] = 2.4 × 10^{14} molec cm^{-3}, [HCHO] = 9 × 10^{16} molec cm^{-3}, 1000 µs after HO_2 formation. The spectrum shape agrees with Figure 4.4, but the absolute absorbance is very low, resulting in a noisy spectrum.

HMP A-X spectrum

Figure 4.9 shows the A-X spectrum of HMP over the range 7100–8000 cm^{-1}. The reported spectrum is a composite of spectra taken over a period of 3 years (2009–2012) under similar experimental conditions (Table 4.1). Certain regions have been scanned in detail, these will be shown later in this section. In general, each point in the spectrum (0.1 cm^{-1} step size) has 3.2 s of averaging.

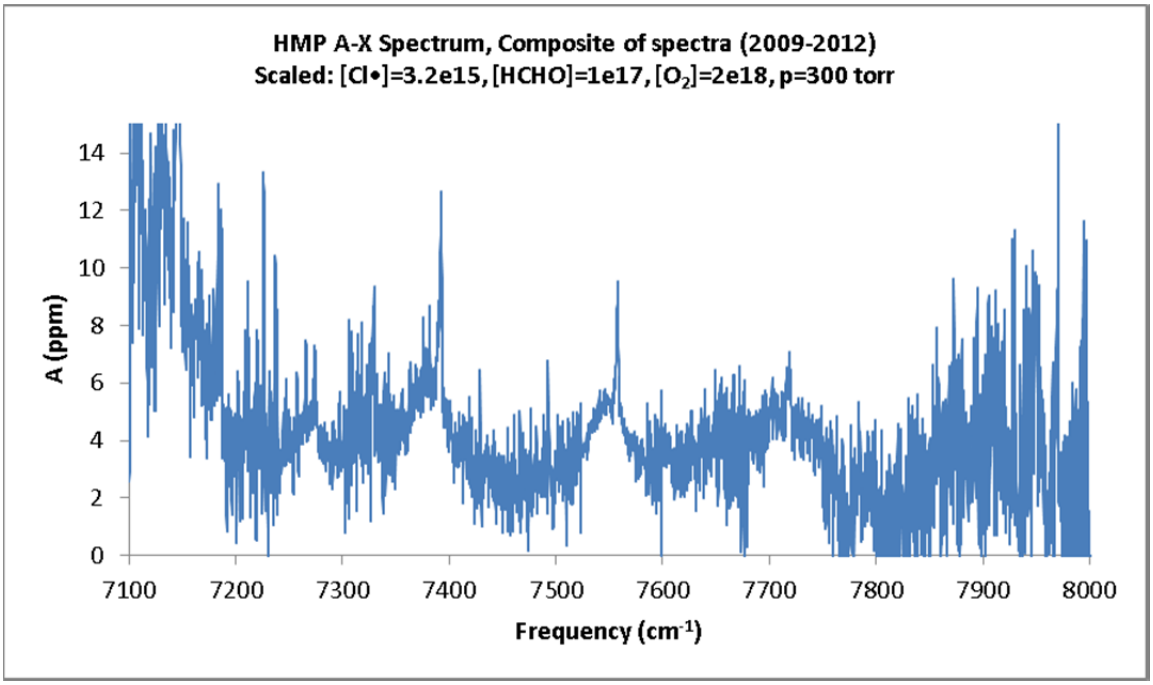

Figure 4.9. Cavity ringdown spectrum of the A-X electronic transition for the hydroxymethylperoxy radical ($HOCH_2OO•$, HMP). We observe clear bandheads of HMP at 7275 cm^{-1} (15_1^0), 7391 cm^{-1} (0_0^0), 7561 cm^{-1} (15_0^1), and 7719 cm^{-1} (15_0^2) that are assigned to HMP. Peaks at 7146, 7185, 7930, and 7975 cm^{-1} are assigned to HO_2.

We immediately note seven peaks that belong to HO_2:[54] 7146, 7185, 7230, 7266, 7330, 7930, and 7975 cm^{-1}. The first two peaks are part of the A-X origin, while the third and fourth peaks are part of the combination band with the OO stretch. The large intensities of the peaks close to the HO_2 transitions (7029, 8050 cm^{-1})[54] prevents us from making meaningful observations in our spectrum at frequencies less than 7200 cm^{-1} or greater than 7900 cm^{-1}.

Despite interference from HO_2, we observe four clean absorption bands in the rest of the spectrum. These bands are located at 7275, 7391, 7561, and 7719 cm^{-1}. Figure 4.10 shows these bands in detail.

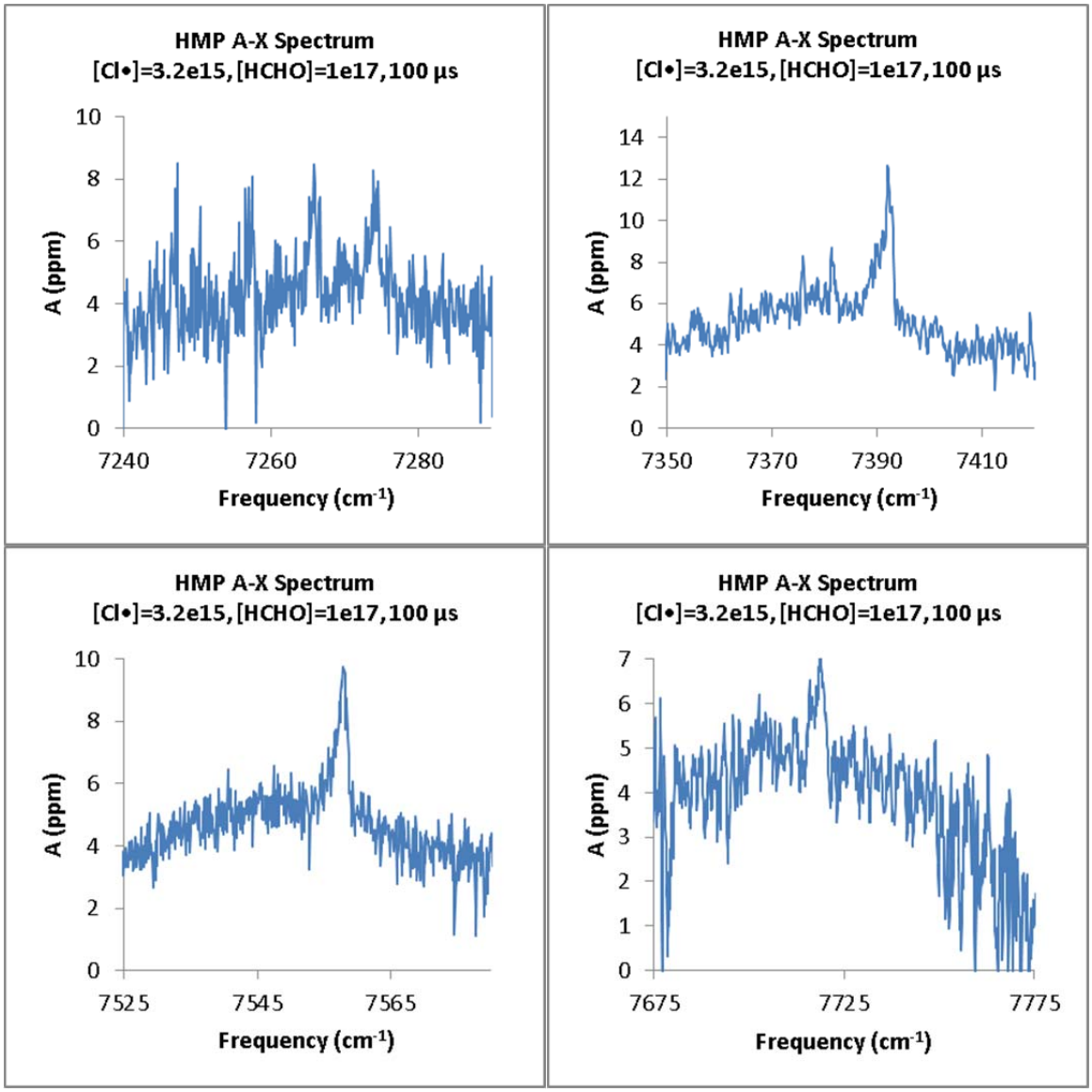

Figure 4.10. Cavity ringdown spectra of individual HMP A-X bands (from Figure 4.8). We assign these bands to HMP on the basis of simulated spectra, our quantum chemistry calculations (Chapter 5) and our kinetics studies (Chapter 6). We assign the bands as: 7275 cm^{-1} (15_1^0), 7391 cm^{-1} (0_0^0), 7561 cm^{-1} (15_0^1), and 7719 cm^{-1} (15_0^2).

We have many pieces of evidence that support assignment of these bands to HMP. First, the kinetics of these bands (discussed in detail in Chapter 6) are consistent with each other, and do not match the kinetics of the HO_2 peaks. Figure 4.11 compares the kinetics of the 7561 cm^{-1} peak to the simulation presented in Figure 4.2. The left panel is measured to the red of the bandhead, and is subject to more noise near the peak

absorption. The right panel is measured at the peak absorption, and is the best measure of the kinetics of the peak. The simulation and observed absorbances are in excellent agreement with each other.

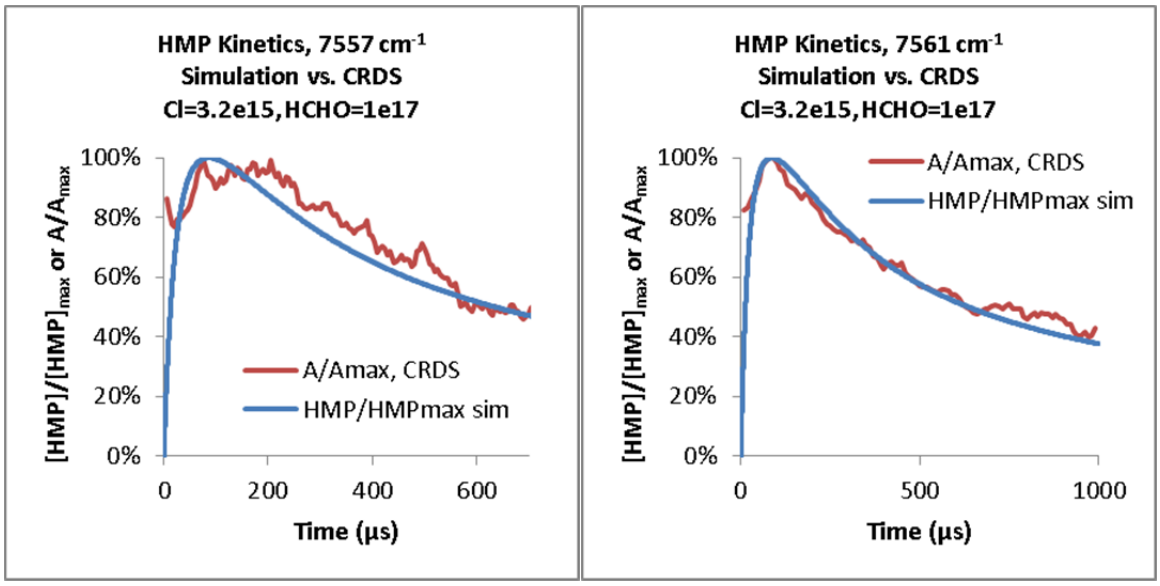

Figure 4.11. Comparison of experimentally measured HMP kinetics (CRDS, 15_0^1 band at 7561 cm^{-1}) to the kinetics simulation presented in Figure 4.2. The left panel was measured to the red of the peak absorbance (7557 cm^{-1}), while the right panel was measured at the bandhead peak. We observe excellent agreement between the experiment and simulation, supporting our assignment of the band to HMP. The other bands (7275, 7391, 7719 cm^{-1}) show similar kinetics (shown in Chapter 6).

The second piece of information supporting assignment of these bands to HMP is the calculated band positions according to quantum chemistry calculations (presented in detail in Chapter 5). Table 4.4 summarizes the A-X transition frequency and anharmonic vibrational modes of HMP in the X and A states. The transition frequency was calculated at CCSD/6-31+G(d,p), and the anharmonic frequencies were calculated at B3LYP/6-31+G(d,p). (Justification of these choices are given in Chapter 5.) These calculations were carried out in Gaussian 09W[121] using the procedures described in Appendix C. Note that mode 15 is the OOCO torsion of HMP, and is the lowest

frequency vibrational mode. We observe excellent agreement between the calculated band positions and observed band positions.

Table 4.4 Comparison of observed transition and torsional frequencies to quantum chemistry predictions for HMP.

	Quantum Chemistry	CRDS	Difference
A-X Transition CCSD/6-31+G(d,p)	7424 cm^{-1}	7391 cm^{-1}	33 cm^{-1}
ν_{15} (X) B3LYP/6-31+G(d,p)	110 cm^{-1}	116 cm^{-1}	6 cm^{-1}
ν_{15} (A) B3LYP/6-31+G(d,p)	168 cm^{-1}	170 cm^{-1}	2 cm^{-1}
$2\nu_{15}$ (A) B3LYP/6-31+G(d,p)	334 cm^{-1}	328 cm^{-1}	6 cm^{-1}

Finally, we can simulate the A-X bands using PGopher[120] and compare to our experiment. We use the geometries and anharmonic rotational constants from our B3LYP/6-31+G(d,p) quantum chemistry calculations. The dipole derivative was estimated as the change in electron density of the OO• π* orbital (most relevant to characteristic peroxy radicals). Figure 4.12 compares the four observed bands (7275, 7391, 7561, 7719 cm^{-1}) to simulations of 15_1^0, 0_0^0, 15_0^1, and 15_0^2 respectively. Despite the high noise level in the 7275 cm^{-1} and 7719 cm^{-1} bands, we observe excellent agreement between the simulations and observed bands.

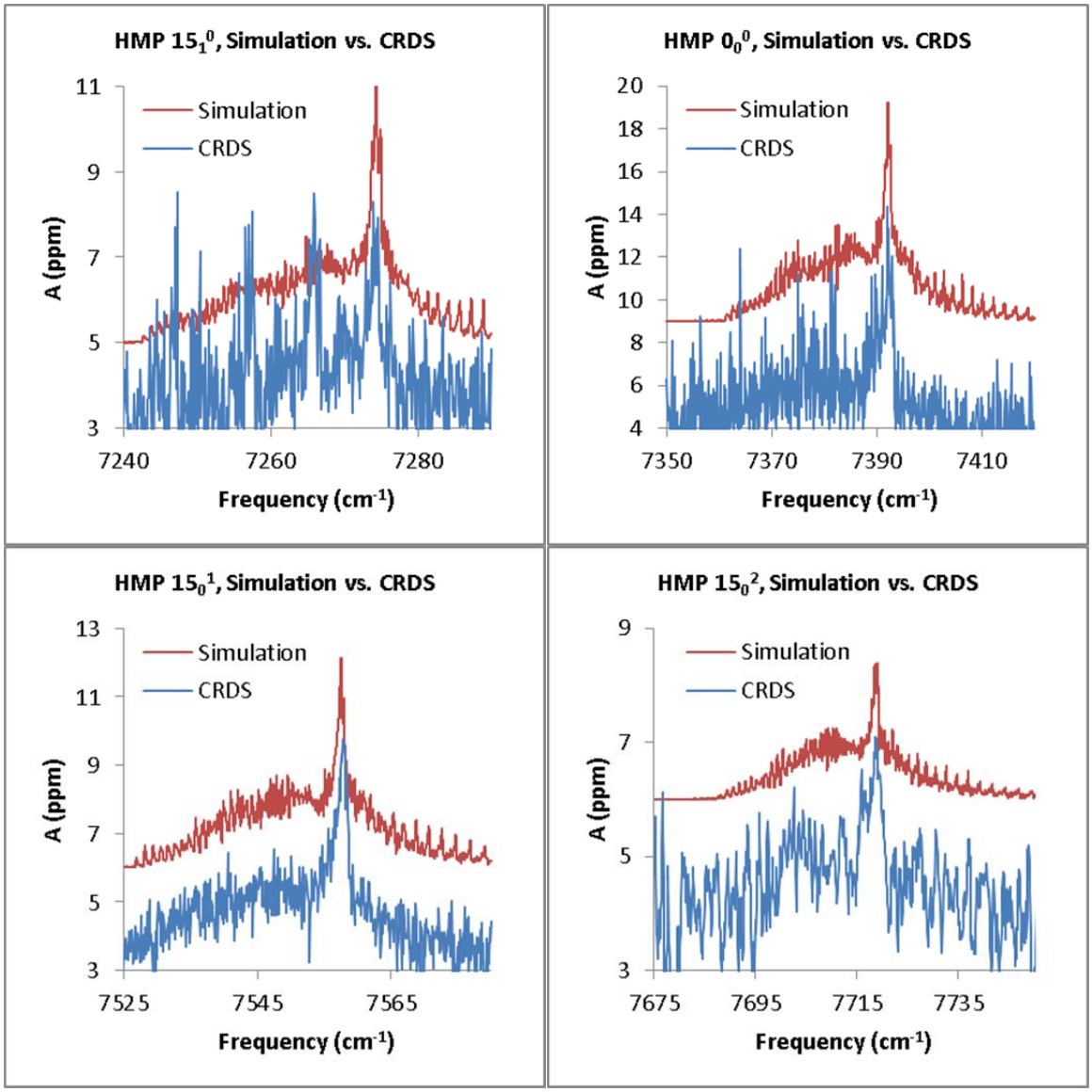

Figure 4.12. Comparison of observed A-X bands of HMP to simulation at B3LYP/6-31+G(d,p), anharmonic rotational constants. Shown above are the bands at 7275 cm^{-1} (15_1^0), 7391 cm^{-1} (0_0^0), 7561 cm^{-1} (15_0^1), and 7719 cm^{-1} (15_0^2).

Given the agreement between our CRDS experiment and theory for the kinetics, position, and shape of each spectroscopic band, we assign the observed bands at 7275, 7391, 7561, and 7719 cm^{-1} to electronic transitions of HMP. The band at 7391 cm^{-1} is assigned as the electronic origin 0_0^0, 7275 cm^{-1} as the OOCO torsion hot band 15_1^0,

7561 cm^{-1} as the OOCO torsion combination band 15^1_0, and 7719 cm^{-1} as the OOCO torsion overtone combination band 15^2_0.

Similar to the ν_1 band, we can estimate the absorption cross sections of the A-X bands in Figure 4.9. Since we do not have a theoretical prediction of the integrated absorbance, we must rely on the kinetics modeling to provide an estimate of [HMP] (3.5×10^{14} molec cm^{-3}). Figures 4.13 and 4.14 show the estimated cross sections for the A-X bands of HMP. We observe peak cross sections on the order 10^{-21}–10^{-20} cm^2 $molec^{-1}$ for the four A-X bands, in reasonable agreement with Melnik's experimentally determined cross section for ethylperoxy (5.29×10^{-21} cm^2 $molec^{-1}$).[115]

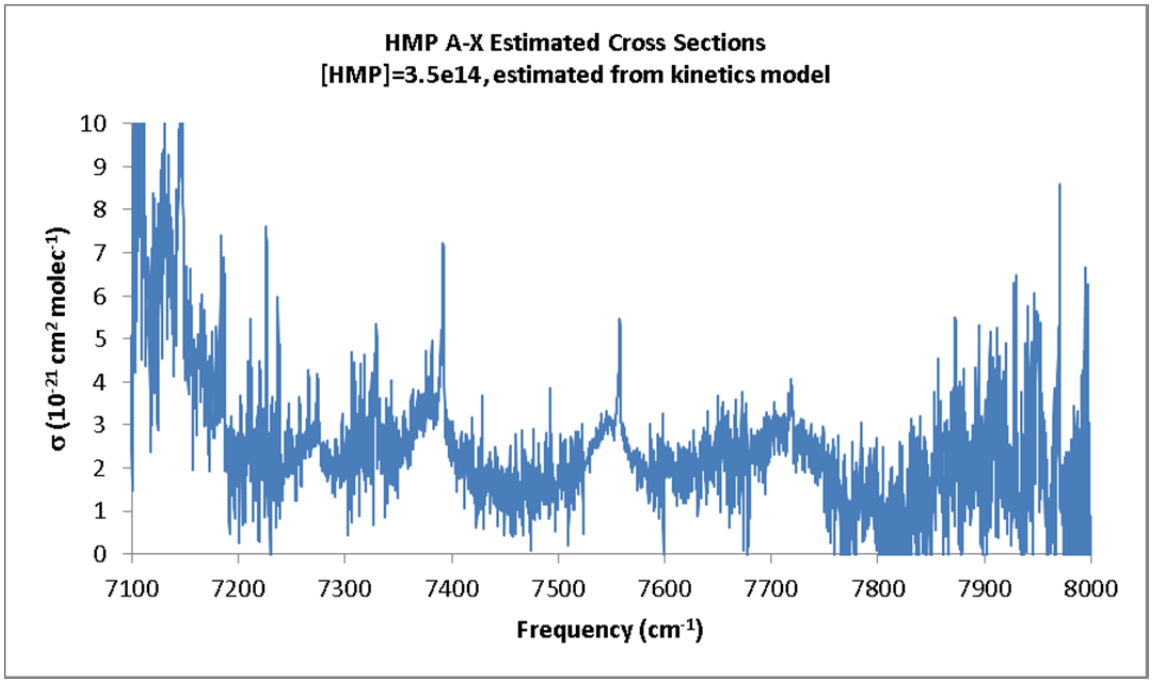

Figure 4.13. Absorption cross sections for the A-X region of HMP. The concentration of absorber used (3.5×10^{14} molec cm^{-3}) was taken to be [HMP] from the kinetics model (Figure 4.2).

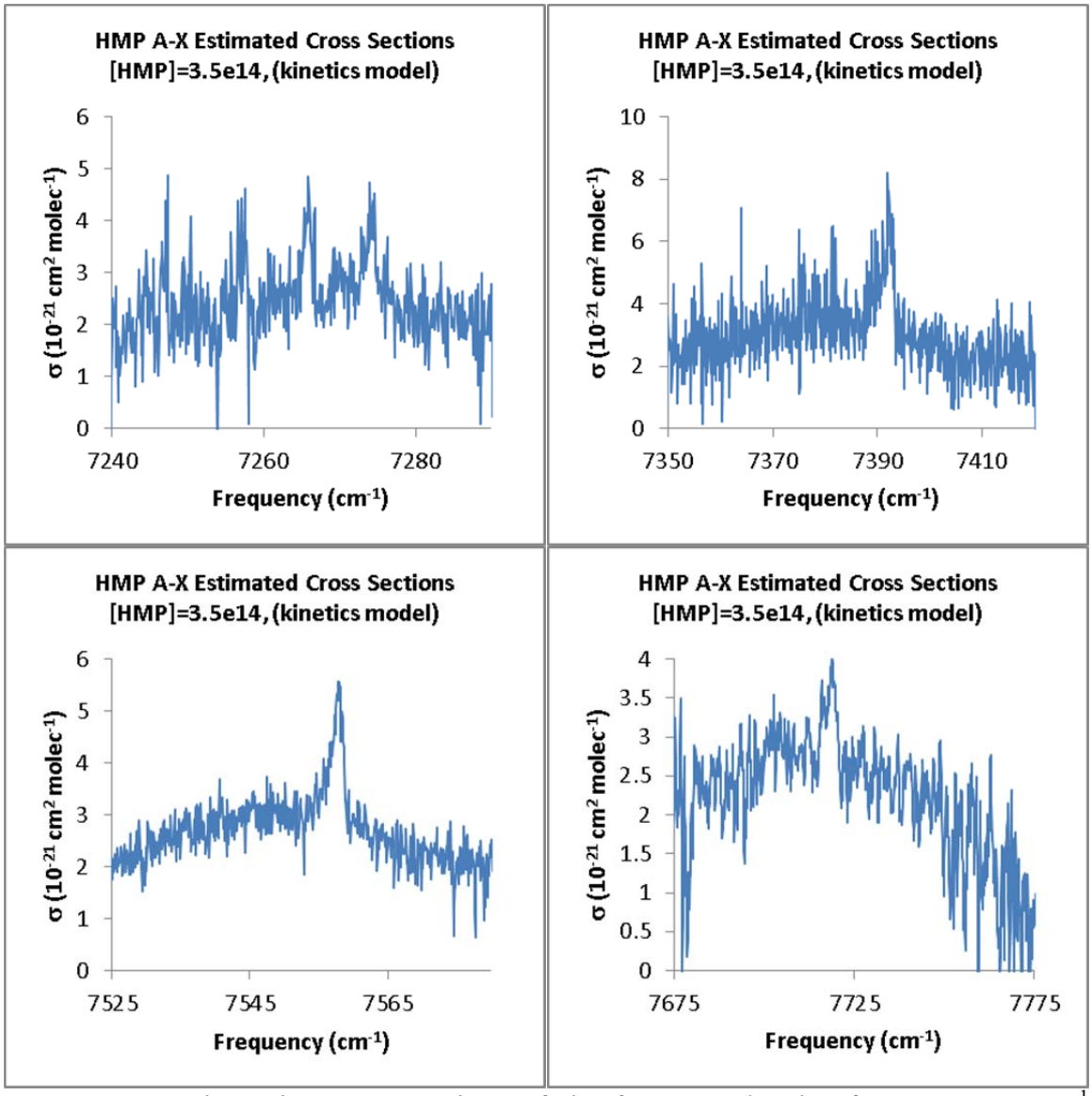

Figure 4.14. Absorption cross sections of the four A-X bands of HMP: 7275 cm^{-1} (15_1^0), 7391 cm^{-1} (0_0^0), 7561 cm^{-1} (15_0^1), and 7719 cm^{-1} (15_0^2). The [HMP] used (3.5×10^{14} molec cm^{-3}) was taken from the kinetics model (Figure 4.2).

Discussion

Comparison of HMP ν_1 Spectrum to Methanol and Ethanol

Figure 4.15 compares the subtracted ν_1 band of HMP (Figure 4.6) to reference spectra of methanol and ethanol.[120] The reference spectra have been smoothed to 1 cm^{-1}, the linewidth of our mid-IR light (Chapter 2).

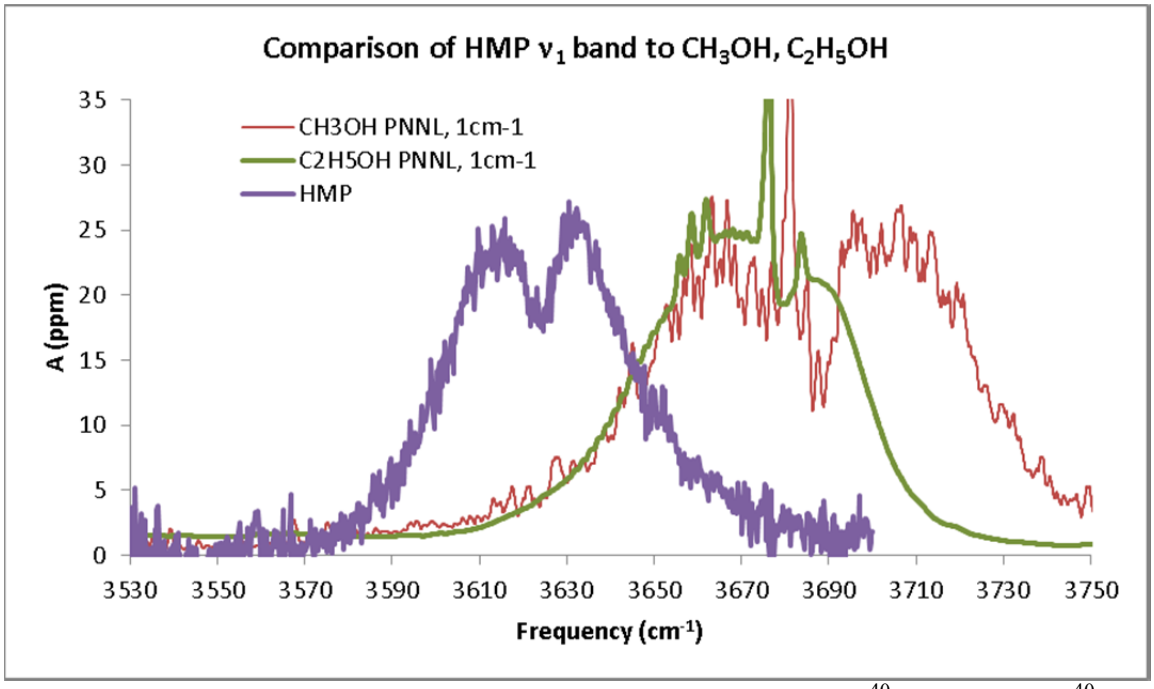

Figure 4.15. ν_1 (OH stretch) spectra of HMP (Figure 4.6), CH_3OH,[40] and C_2H_5OH.[40] The reference spectra for CH_3OH and C_2H_5OH have been smoothed to 1 cm^{-1} in order to match the linewidth of the HMP spectrum.

The shape of the HMP ν_1 band is similar to both methanol and ethanol. The FWHM of HMP (60 cm^{-1}) is equal to ethanol, but narrower than methanol (90 cm^{-1}), consistent with the difference in rotational constants between the three molecules. Second, the peak of HMP is red shifted from the alcohols by 55–60 cm^{-1}. This is consistent with formation of a weak intramolecular hydrogen bond in HMP (discussed in detail in Chapter 5).

Despite the difference in band positions, the similarities in band shapes give us more confidence in our assignment of the observed absorption to the ν_1 band of HMP.

Comparison of HMP A-X Spectrum to Methylperoxy

We can also compare the A-X spectrum of HMP to the A-X spectrum of methylperoxy obtained by Chung et al.[122] Figure 4.16 shows these two spectra. Chung

generates methylperoxy radicals by photolysis of acetone at 193 nm. Based on their reported experimental conditions, $[CH_3OO\bullet] = 7 \times 10^{15}$ molec cm^{-3}, with a photolysis length of 13 cm.

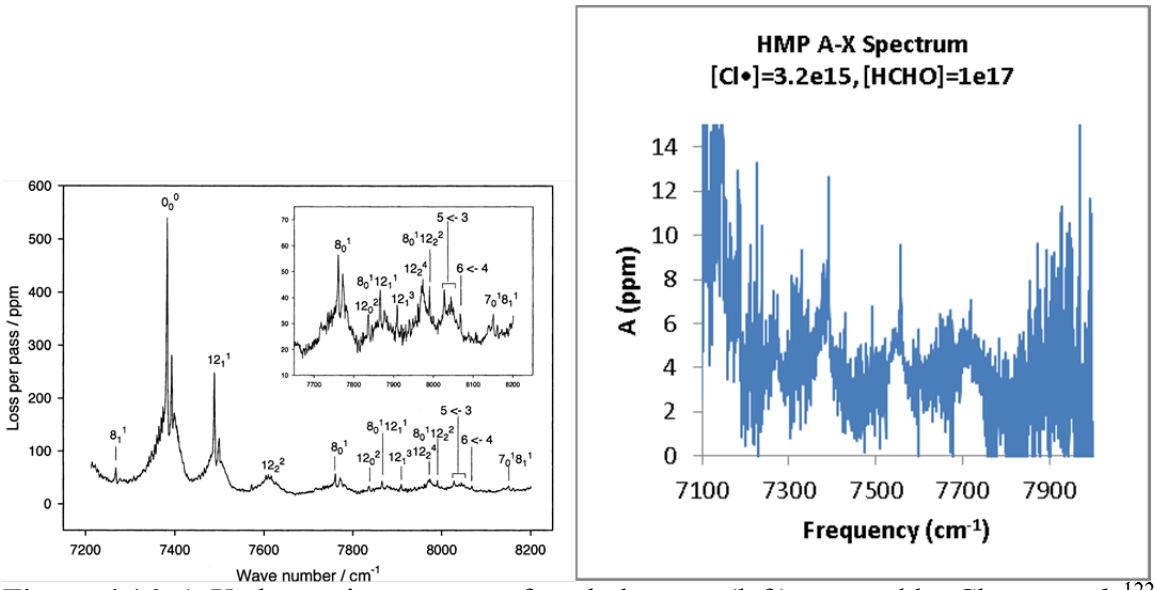

Figure 4.16. A-X electronic spectrum of methylperoxy (left) reported by Chung *et al.*,[122] and our A-X spectrum of HMP (right). Left panel reprinted with permission from Chung *et al*.[122] Copyright 2007, American Institute of Physics.

Chung's spectrum differs from our spectrum in two ways. First, Chung does not subtract out the mirror reflectivity (50 ppm). Second, Chung makes use of $[CH_3OO] \times L_{phot}$ a factor of 45 higher than our expected [HMP] × L_{phot} , consequently making the absolute absorbances of each spectrum on different scales. Thus, the observed 0_0^0 peak absorbance of 550 ppm in Chung's spectrum would be equivalent to a peak absorbance of 11 ppm in our spectrum. We therefore observe good agreement in the linestrength of the pure A-X electronic transition between HMP and $CH_3OO\bullet$. Likewise, there is good agreement between the torsional overtone bands (12_0^2 in CH_3OO, 15_0^2 in HMP).

However, there are major differences between the two spectra over the range 7200–7600 cm^{-1}. In the CH_3OO spectrum, a sequence band involving the methyl torsion, 12_1^1, is observed at 7480 cm^{-1}. The pure methyl torsion band, 12_0^1, is not observed. In contrast, we do not observe the analogous sequence band 15_1^1 in the HMP spectrum, but we do see the "hydroxymethyl" torsion analog (OOCO torsion band) 15_0^1 at 7561 cm^{-1}. Similarly, Chung does not observe the torsional hot band 12_1^0 in the CH_3OO spectrum, although we see the analogous 15_1^0 band of HMP. These differences are likely due to the difference in molecular symmetry between HMP (C_1) and CH_3OO• (C_s), and differences in the dipole moment due to the hydroxyl group in HMP.

Conclusions

In this chapter, we have reported the first detection of the ν_1 (OH stretch) vibrational and A-X electronic spectra of the hydroxymethylperoxy radical ($HOCH_2OO$•, HMP), the product of HO_2 + HCHO. The ν_1 spectrum is broad, with strong, structureless P and R branches. Under the experimental conditions used for the ν_1 spectrum, we observe relatively little interference from HCOOH and H_2O_2, in good agreement with our predictions from kinetics modeling and chemistry analysis. We observe multiple electronic transitions corresponding to the pure A-X transition, and combination/hot bands with the OOCO torsion. Both the ν_1 and A-X bands agree well with simulation and spectra of similar molecules.

Assignment of the ν_1 and A-X bands were supported by quantum chemistry calculations and kinetics results. These topics are explored in detail in Chapters 5 and 6, respectively.

Acknowledgements

We thank Aileen O. Hui and Kathryn A. Pérez for assistance with calibration of the formaldehyde gas line, and Ralph H. Page for improvements to the optical setup. The experiments performed in this chapter were funded under NASA Upper Atmosphere Research Program Grants NAG5-11657, NNG06GD88G, and NNX09AE21G2, California Air Resources Board Contract 03-333 and 07-730, National Science Foundation CHE-0515627, and a Department of Defense National Defense Science and Engineering Graduate Fellowship (NDSEG).